

Primordial non-Gaussianity from the 21 cm Power Spectrum during the Epoch of Reionization

Shahab Joudaki,¹ Olivier Doré,^{2,3} Luis Ferramacho,^{4,5} Manoj Kaplinghat,¹ and Mario G. Santos⁶

¹*Center for Cosmology, Dept. of Physics & Astronomy, University of California, Irvine, CA 92697*

²*Jet Propulsion Laboratory, California Institute of Technology, Pasadena, CA 91109*

³*California Institute of Technology, Pasadena, CA 91125*

⁴*CNRS, IRAP, 14 Avenue Edouard Belin, F-31400, Toulouse, France*

⁵*Université de Toulouse, UPS-OMP, IRAP, Toulouse, France*

⁶*CENTRA, Departamento de Física, Instituto Superior Tecnico, 1049-001 Lisboa, Portugal*

(Dated: January 20, 2013)

Primordial non-Gaussianity is a crucial test of inflationary cosmology. We consider the impact of non-Gaussianity on the ionization power spectrum from 21 cm emission at the epoch of reionization. We focus on the power spectrum on large scales at redshifts of 7 to 8 and explore the expected constraint on the local non-Gaussianity parameter f_{NL} for current and next-generation 21 cm experiments. We show that experiments such as SKA and MWA could measure f_{NL} values of order 10. This can be improved by an order of magnitude with a fast-Fourier transform telescope like Omniscope.

Introduction. An inflationary epoch in the early universe [1, 2] has been established as a solution to the cosmological horizon and flatness problems over the past three decades, most recently through high-precision measurements of the cosmic microwave background (CMB) by the Wilkinson Microwave Anisotropy Probe (WMAP) [3]. The inflationary hypothesis predicts an epoch of exponential growth lasting at least 60 e-folds resulting in almost Gaussian scale-invariant density perturbations [4].

A powerful mechanism to distinguish between inflation models is the amplitude and scale dependence of mild non-Gaussianity in perturbations of the primordial density field. Canonical single field inflation models predict primordial non-Gaussianity (bispectrum) of the local form $|f_{\text{NL}}| \ll 1$ [5, 6], while evolution after inflation generates non-local bispectrum with effective $f_{\text{NL}} = \mathcal{O}(1)$ [7–9]. The best current constraints of ± 25 on local f_{NL} [10, 11] are from WMAP data. A future measurement of $f_{\text{NL}} = \mathcal{O}(1)$ could reveal the existence of physics beyond the standard single field slow-roll inflationary scenario.

We show that radio interferometric probes [12–15] of 21 cm emission from spin-flip transitions of neutral hydrogen at the epoch of reionization (EoR) [16] can result in constraints on f_{NL} at the same level as Planck [17], and less than unity in the most optimistic experimental proposal. Previous studies have explored primordial non-Gaussianity in the bispectrum of ideal 21 cm experiments prior to the EoR [18, 19]. In this work, we consider scale dependent bias in the power spectrum of ionized hydrogen resulting from departures from Gaussian initial conditions [20, 21]. Our constraints from 21 cm emission do not require an ionization-clean cosmology, i.e., a priori knowledge of the spectrum of fluctuations in the ionized fraction.

The rest of the letter is arranged as follows. We first

quantify the influence of non-Gaussianity of the local form on the 21 cm power spectrum, and then test this via numerical simulations of the ionization distribution. We review the assumed noise properties of LOFAR [12], MWA [14], SKA [13], and Omniscope [15], and forecast constraints on f_{NL} based on a Fisher matrix analysis. For these forecasts, we fix the parameters of our fiducial flat Λ CDM model to agree with WMAP7 [22].

Effect of Non-Gaussianity on the 21 cm Power Spectrum. We decompose the 21 cm power spectrum at redshift z in terms of its angular dependence [23], given by $\mu = \hat{\mathbf{k}} \cdot \hat{\mathbf{n}} = \cos(\theta)$, where θ is the angle between wavevector \mathbf{k} and line of sight (LOS) vector \mathbf{n} :

$$P_{\Delta T}(\mathbf{k}, z) = \mathcal{P}_{\delta\delta}(k, z) - 2\mathcal{P}_{x\delta}(k, z) + \mathcal{P}_{xx}(k, z) + 2[\mathcal{P}_{\delta\delta}(k, z) - \mathcal{P}_{x\delta}(k, z)]\mu^2 + \mathcal{P}_{\delta\delta}(k, z)\mu^4. \quad (1)$$

We define $\mathcal{P}_{\delta\delta} \equiv \tilde{T}_b^2 \bar{x}_H^2 P_{\delta\delta}$ [24], where $P_{\delta\delta}$ is the linear matter power spectrum, numerically obtained from a modified version of CAMB [25], \bar{x}_H is the mean neutral fraction of hydrogen such that the ionized fraction $\bar{x}_i \equiv 1 - \bar{x}_H$, and $\tilde{T}_b(z = 7.5) \simeq 0.026$ K is the spatially averaged brightness temperature. We consider only large enough scales ($k < 0.15/\text{Mpc}$) such that the ionization power spectrum $\mathcal{P}_{xx} \simeq b_x^2 \mathcal{P}_{\delta\delta}$ and the ionization-density cross spectrum $\mathcal{P}_{x\delta} \simeq b_x \mathcal{P}_{\delta\delta}$, where b_x is the bias of ionized regions. Our numerical simulations in Fig. 1 show that this is an excellent approximation.

We define \mathbf{u} as the Fourier dual of $\Theta \equiv \theta_i \hat{e}_i + \theta_j \hat{e}_j + \Delta f \hat{e}_k$, where θ_i and θ_j encode the angular location on the 2D sky, and Δf measures the difference in frequency. The 21 cm power spectrum is extended to \mathbf{u} -space in which measurements are made:

$$P_{\Delta T}(\mathbf{u}, z) = P_{\Delta T}(\mathbf{k}, z) / (\chi^2(z)y(z)), \quad (2)$$

where $\chi(z)$ is the comoving distance to a given redshift, $y(z) = \lambda_{21}(1+z)^2/H(z)$ translates between intervals in

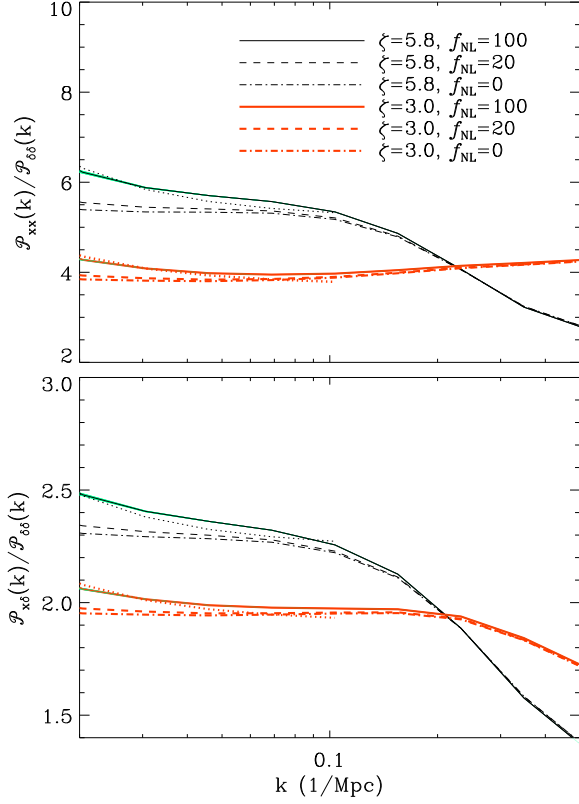


FIG. 1. Ionization power spectra with non-Gaussianity of the local form from numerical simulations. We show $f_{\text{NL}} = (0, 20, 100)$ (dot-dashed, dashed, solid) for efficiency $\zeta = (5.8, 3.0)$ (thin black, thick red) at $z = 7.5$, where $\bar{x}_H = (0.50, 0.75)$. For $f_{\text{NL}} = 100$ cases, sample variance from simulations is in form of green bands about the mean, and analytical fits corresponding to $\bar{\delta}_B = 1$ are in dotted lines.

frequency and distance, and $\lambda_{21} = \lambda(z)/(1+z) = 0.21$ m. We convert between u and k spaces via $u_\perp = \chi(z)k_\perp = 2\pi L/\lambda(z)$, where L is the baseline, and $u_\parallel = y(z)k_\parallel$.

Given non-Gaussianity of the local form, Bardeen's gauge invariant potential field Φ is related to a pure gaussian random field ϕ at nonlinear order [7, 26]:

$$\Phi_{\text{NG}}(\mathbf{x}) = \phi(\mathbf{x}) + f_{\text{NL}}(\phi^2(\mathbf{x}) - \langle \phi^2 \rangle). \quad (3)$$

In the high-peaks formalism f_{NL} influences biased tracers of the underlying matter distribution as a scale dependent correction to the large scale bias [20, 21]. This enters as $\mathcal{P}_{x\delta}/\mathcal{P}_{\delta\delta} = b_x + \Delta b_x$, $\mathcal{P}_{xx}/\mathcal{P}_{\delta\delta} = (b_x + \Delta b_x)^2$, with

$$\Delta b_x(k, z) = 3(b_x - 1)f_{\text{NL}}\Omega_m H_0^2 \bar{\delta}_B / (D(z)k^2 T(k)), \quad (4)$$

where H_0 is the Hubble constant, Ω_m is the present density parameter of matter, $D(z)$ is the linear growth function of density perturbations, and $T(k)$ is the transfer function relating present and primordial power spectra. The quantity $\bar{\delta}_B$ is the average critical collapse density of HII regions [27]. We leave the bias b_x as a free parameter, although b_x , $\bar{\delta}_B$, and \bar{x}_H would all be related in a given

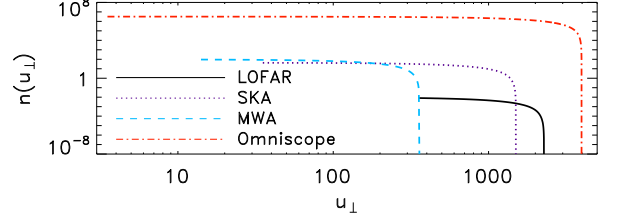


FIG. 2. Number density of baselines for LOFAR (solid), SKA (dotted), MWA (dashed), and Omniscience (dot-dashed).

| Experiment | N_{ant} | L_{min} (m) | FOV (deg ²) | A_e (m ²) |
|-------------|------------------|----------------------|-------------------------|-------------------------|
| LOFAR | 32 | 100 | $2 \times \pi 2.4^2$ | 590 |
| MWA | 500 | 4.0 | $\pi 16^2$ | 13 |
| SKA | 1400 | 10 | $\pi 8.6^2$ | 45 |
| Omniscience | 10^6 | 1.0 | 2.1×10^4 | 1.0 |

TABLE I. Experimental specifications for the telescopes. The antenna number only account for those inside the nucleus and core (e.g. for SKA we use 1400 of a total 7000 antennae). The system temperature $T_{\text{sys}} = 390$ K, bandwidth is 6 MHz, observation time is 4000 hours, and effective area at $z = 7.5$.

model of reionization. The scale-dependence of the bias in Δb_x is clearly evident in the ionization spectra from our simulations in Fig. 1. We find that $\bar{\delta}_B \sim 1$ fits the large-scale f_{NL} induced rise to the ionization spectrum.

Numerical Simulations with Non-Gaussian Initial Conditions. We perform simulations of the ionization distribution during the EoR for $f_{\text{NL}} = (0, 20, 100)$ and ionization efficiency $\zeta = (3.0, 5.8)$, in a box of co-moving length 3000 Mpc, with a modified version of SimFast21 [28, 29]. The initial matter density field is computed from the Poisson equation with non-Gaussian gravitational potential $\Phi_{\text{NG}}(\mathbf{k})$. We show the spectra from these simulations in Fig 1, from which $\bar{\delta}_B \sim 1$.

We compare this result to the theoretical prediction. The critical density for collapse of an ionized region of mass m is obtained from the collapse fraction f_{coll} [27]:

$$\delta_B(m, z) = \delta_c - K(\zeta)\sqrt{2(\sigma^2(m_{\text{min}}, z) - \sigma^2(m, z))}, \quad (5)$$

where $\delta_c \approx 1.68$ is the critical collapse density of matter, $\sigma^2(m, z)$ is the variance of the density fluctuations, and m_{min} corresponds to a virial temperature of 10^4 K. Moreover, $K(\zeta) = \text{erf}^{-1}(1 - \zeta^{-1})$, where $\zeta = m_{\text{ion}}/m_{\text{gal}}$ is the ionization efficiency [27]. We evaluate $\bar{\delta}_B$ as an average over the fraction of space filled by HII bubbles as in Ref. [27]. Given this prescription, we find $\bar{\delta}_B = 1.1$ (less than δ_c as $\zeta > 1$), matching the simulation results well. This becomes $\bar{\delta}_B = 1.2$ if we only average over the mass function. For simplicity, we fix $\bar{\delta}_B = 1$.

As noted earlier, the bias b_x , collapse threshold $\bar{\delta}_B$, and \bar{x}_H are expected to be interrelated in a given reionization scenario. This is evident in Fig. 1, where we see that a factor of 2 change in ζ changes the bias by about 15%. This change is subdominant to the impact of \bar{x}_H (linear

function of ζ) on the 21 cm power spectrum. In a more optimistic scenario, one could envision constraining \bar{x}_H (or ζ) together with f_{NL} without b_x as a free parameter. We also considered the impact of variations in \bar{x}_H and f_{NL} on $\bar{\delta}_B$. Changing \bar{x}_H by a factor of two only affects $\bar{\delta}_B$ by 8% given $(1 - \bar{x}_H) = \zeta f_{coll}$. Nonzero f_{NL} skews $\bar{\delta}_B(m, z)$ through its influence on f_{coll} . Using the results of Ref. [30], we estimate $\bar{\delta}_B$ is only perturbed by 4% even for $f_{NL} = 100$. This is because the sensitivity to f_{NL} increases with mass, while the mass scales that contribute a majority of the integral over the mass function lie within an order of magnitude of the minimum halo mass.

21 cm Noise Power Spectrum. The noise power spectrum of 21 cm fluctuations is expressed as [24, 31]

$$P_N(u_\perp, z) = (\lambda^2(z) T_{sys}(z) / A_e(z))^2 / (t_0 n(u_\perp)), \quad (6)$$

where the sky-dominated system temperature $T_{sys} \simeq 280((1+z)/7.4)^{2.3}$ K [32], t_0 is the total observation time, and $A_e(z) \propto \lambda^2(z)$ is the effective collecting area (listed in Table I). Here, $n(u_\perp)$ encodes the number density of baselines shown in Fig. 2, computed as the autocorrelation of the array density for each of the surveys.

The array distributions are composed of a nucleus with full coverage fraction and a core with power law r^{-2} . The nucleus radius is $R_n = \sqrt{\eta N_{ant}} / (\rho_0 \pi)$, where ρ_0 is the 2D array density of the nucleus, and N_{ant} is the number of antennae of each experiment (see Table I). The core radius is by construction $R_c = R_n \exp((1 - \eta)/(2\eta))$ [24]. The most optimal choice of η for constraints on f_{NL} depends on the particular experiment and bandwidth B considered, but for comparison with prospective constraints on other cosmological parameters in Table V of Ref. [24], we choose $\eta = 0.8$ for [LOFAR, MWA, SKA], whereas all of Omniscopes's antennae lie in the nucleus.

We assume residual foregrounds can be ignored beyond $k_\parallel \geq 2\pi/(yB)$ [31], but also consider the case where foregrounds can be removed on larger scales (Fig 3).

Fisher Matrix Forecasts. We evaluate the prospective constraints on f_{NL} from the 21 cm power spectrum at the EoR via the Fisher matrix formalism. The summation involves pixels in (k_\perp, k_\parallel) of thickness $(\epsilon_\perp, \epsilon_\parallel) = (\Delta k_\perp / k_\perp, \Delta k_\parallel / k_\parallel) = (0.1, 0.1)$:

$$\mathbf{F}_{ab} = \sum_{\text{pixels}} \frac{1}{[\delta P_{\Delta T}(\mathbf{u})]^2} \left(\frac{\partial P_{\Delta T}(\mathbf{u})}{\partial p_a} \right) \left(\frac{\partial P_{\Delta T}(\mathbf{u})}{\partial p_b} \right). \quad (7)$$

We have verified that our forecasts are robust to variations in the step sizes of parameter space and \mathbf{k} -space. The measurement error consists of the sum of the sample variance and thermal detector noise over half-space [31]:

$$\delta P_{\Delta T}(\mathbf{u}) = (P_{\Delta T}(\mathbf{u}) + P_N(u_\perp)) / \sqrt{N_m}. \quad (8)$$

The number of modes falling in each pixel is given by $N_m = 2\pi k_\perp \Delta k_\perp \Delta k_\parallel V(z) / (2\pi)^3$, such that the volume

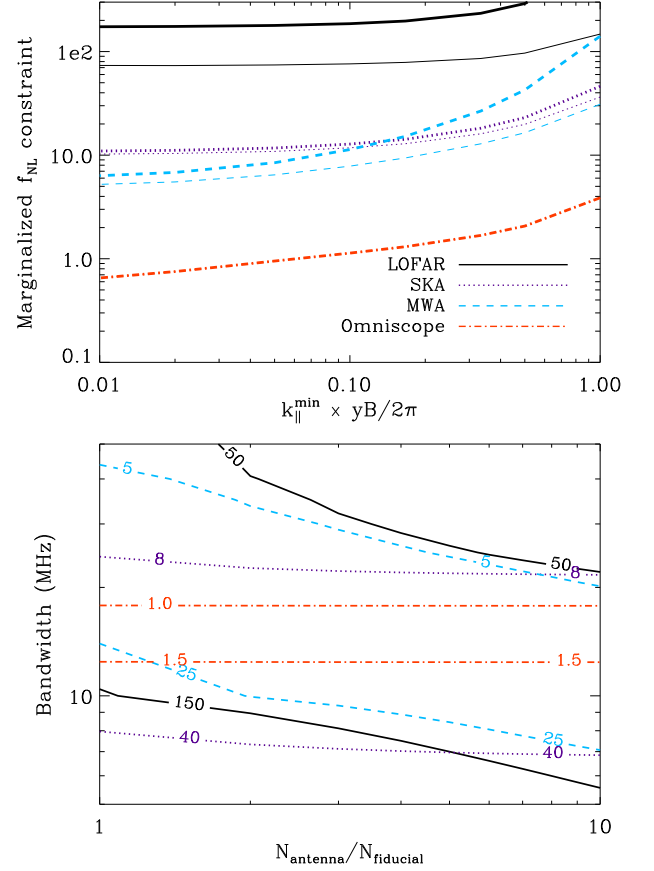


FIG. 3. *Top:* Marginalized f_{NL} constraints for cases with noise (thick) and without noise (thin), which overlap for Omniscopes. We consider a bandwidth of 6 MHz, but assume foregrounds can be removed on scales larger than $k_\parallel = 2\pi/(yB)$. *Bottom:* Marginalized f_{NL} constraints as function of bandwidth and number of antennae. The bandwidth limits the number of modes and largest scale probed along the LOS (via the survey volume $V \propto B$ and $k_\parallel^{\min} \propto 1/B$), whereas a larger number of antennae for fixed array density increases the survey resolution and number of perpendicular modes (via $n(u_\perp)$, on large scales $\propto N_{ant}$, and $u_\perp^{\max} \propto \sqrt{N_{ant}}$). The color coding is the same as for the top panel.

sampled $V(z) = \chi^2 yB \times \text{FOV}$, where FOV denotes the field of view of the telescope (often equal to λ^2/A_e).

For a single redshift bin at $z = 7.5$, we fiducially let $b_x = 2.3$ and $\bar{x}_H = 0.5$. The bandwidth $B = 6$ MHz limits $k_\parallel^{\min} = 2\pi/(yB) \gtrsim 0.063/\text{Mpc}$ [31], and nonlinearities force $k_\parallel^{\max} \sim 2/\text{Mpc}$. The ranges in k_\perp at the central redshift are $[0.039, 0.25]/\text{Mpc}$ for LOFAR, $[0.0016, 0.040]/\text{Mpc}$ for MWA, $[0.0039, 0.17]/\text{Mpc}$ for SKA, and $[3.9 \times 10^{-4}, 0.44]/\text{Mpc}$ for Omniscopes. However, due to our narrow focus on f_{NL} at the largest scales in which the $1/k^2$ boost becomes significant, in practice, we only keep modes up to $k^{\max} = 0.15/\text{Mpc}$.

Results. In quantifying our constraints on f_{NL} , we fix the underlying cosmology. By only considering large enough scales for which the ratio of the ionization and

matter spectra is constant in a universe without non-Gaussianity, the free parameters in a single redshift bin at $\bar{x}_H = 0.5$ are limited to $(f_{\text{NL}}, b_x, \bar{x}_H)$. With Planck priors on the standard cosmological parameters [17], in particular the matter power spectrum normalization Δ_R^2 , cold dark matter density $\Omega_c h^2$, spectral index n_s , and its running $dn_s/d \ln k$, we find the f_{NL} constraints from [LOFAR, MWA, SKA] are robust to the assumption of a fixed cosmology at the 10% level, while the same level of robustness for Omniscope is achieved after including its constraints on $(n_s, dn_s/d \ln k, \Omega_c h^2)$ from small scales. The constraints on f_{NL} will depend on the fiducial b_x , but we do not explore this issue here.

Fig. 3 (top) shows f_{NL} constrained as function of the minimum LOS wavenumber, limited by the experimental ability to remove foregrounds. Imposing $k_{\parallel}^{\text{min}} = 2\pi/(yB) = 0.063/\text{Mpc}$ [31], we find the constraints for [LOFAR, MWA, SKA, Omniscope] are equal to $\sigma(f_{\text{NL}}) = [700, 100, 50, 4]$, which reduces to $\sigma(f_{\text{NL}}) = [100, 30, 40, 4]$ when instrumental noise is neglected. These constraints improve for telescopes with increased ability to probe larger LOS scales. When arbitrarily large scales along the LOS can be probed, we find $\sigma(f_{\text{NL}}) = [200, 6, 10, 0.6]$, which reduces to $\sigma(f_{\text{NL}}) = [70, 5, 10, 0.6]$ when noise is neglected. The constraints plateau for $k_{\parallel}^{\text{min}} \rightarrow 0$ due to the nonzero k_{\perp}^{min} set by the minimum experiment baseline. As $k_{\parallel}^{\text{min}}$ decreases, our assumed MWA configuration becomes somewhat better than the SKA configuration in constraining f_{NL} due to its smaller minimum baseline, allowing larger scales to be probed by the telescope.

In Fig. 3 (bottom), we consider a minimum LOS scale set by $k_{\parallel}^{\text{min}} = 2\pi/(yB)$, but allow an order of magnitude variation in bandwidth and telescope antenna number. The bandwidth is inversely proportional to the minimum LOS wavenumber and linearly increases the volume probed, whereas larger number of antennae for fixed array density increases the maximum baseline as $\sqrt{N_{\text{ant}}}$ and linearly boosts the baseline density (thereby decreasing the noise). The contours show increased bandwidth is more powerful in the search for f_{NL} , in particular for SKA and Omniscope that have small instrumental noise. This is because their signal-to-noise is already close to the cosmic variance limit, and our power spectrum cutoff at $k = 0.15/\text{Mpc}$ makes us insensitive to the increasing number of small scale modes. Extending the considered modes to scales of $k = 2/\text{Mpc}$ (incorporating modeling of the exponential tail with very strong priors on the new free parameters) improves the constraints by up to factor of 2 for the different experimental configurations.

We have also considered the case where the bias and ionization fraction are fixed. In this scenario, the f_{NL} constraints improve by a factor of 1.5 up to a factor of 10 for the various cases and experiments considered. For the fiducial configurations alone, the f_{NL} constraints improve by factors of 2 (MWA) to 3 (LOFAR, SKA, Omniscope)

when fixing the bias to be a function of the ionization fraction. When only information from scales larger than $k^{\text{max}} = 0.10/\text{Mpc}$ is available (compared to $0.15/\text{Mpc}$ assumed throughout the paper), the constraint on f_{NL} degrades by up to a factor of 2 when marginalizing over b_x and \bar{x}_H , and by up to 30% when b_x and \bar{x}_H are fixed.

Conclusions. The search for a signature of primordial non-Gaussianity is a key test of inflationary theories. Large values for the non-Gaussianity parameter, $f_{\text{NL}} \gg 1$, will rule out standard single field inflationary models. We have considered the impact of primordial non-Gaussianity on the ionization power spectrum from 21 cm emission at the epoch of reionization, which provides an alternative approach to constrain f_{NL} relative to the cosmic microwave background and large-scale structure. We find that f_{NL} can be constrained to an accuracy of order 10 with future 21 cm telescopes like SKA and MWA. This improves by an order of magnitude for a fast-Fourier transform telescope like Omniscope, thereby opening a new window to inflationary physics.

Acknowledgements: We thank A. Amblard, Y. Mao, G. Martinez, M. McQuinn, J. Smidt, and E. Tollerud for useful discussions. MGS acknowledges support by FCT under grant PTDC/FIS/100170/2008. MK acknowledges support by NSF under grant NSF 0855462 at UCI. Part of the research described in this letter was carried out at JPL, Caltech, under contract with NASA.

-
- [1] A. H. Guth, Phys. Rev. D **23**, 347 (1981).
 - [2] A. D. Linde, Phys. Lett. B **108**, 389 (1982).
 - [3] D. N. Spergel *et al.*, Astrophys. J. Suppl. **148**, 175 (2003).
 - [4] N. Bartolo, *et al.*, Phys. Rept. **402**, 103 (2004).
 - [5] J. M. Maldacena, JHEP **0305**, 013 (2003).
 - [6] V. Acquaviva, *et al.*, Nucl. Phys. B **667**, 119 (2003).
 - [7] L. Verde, *et al.*, MNRAS **313**, 141 (2000).
 - [8] M. Liguori, *et al.*, Phys. Rev. D **73**, 043505 (2006).
 - [9] K. M. Smith & M. Zaldarriaga, arXiv:0612571.
 - [10] K. M. Smith, *et al.*, JCAP **0909**, 006 (2009).
 - [11] J. Smidt, *et al.*, Phys. Rev. D **80**, 123005 (2009).
 - [12] <http://www.lofar.org>
 - [13] <http://www.skatelescope.org>
 - [14] <http://www.mwatelescope.org>
 - [15] M. Tegmark & M. Zaldarriaga, PRD **82**, 103501 (2010).
 - [16] S. Furlanetto, *et al.*, Phys. Rept. **433**, 181 (2006).
 - [17] G. Efstathiou, *et al.*, ESA-SCI 1 (2005).
 - [18] A. Cooray, Phys. Rev. Lett. **97**, 261301 (2006).
 - [19] A. Pillepich, *et al.*, Astrophys. J. **662**, 1 (2007).
 - [20] N. Dalal, *et al.*, Phys. Rev. D **77**, 123514 (2008).
 - [21] S. Matarrese & L. Verde, Astrophys. J. **677**, L77 (2008).
 - [22] E. Komatsu *et al.*, Astrophys. J. Suppl. **192**, 18 (2011).
 - [23] R. Barkana & A. Loeb, Astrophys. J. **624**, L65 (2005).
 - [24] Y. Mao, *et al.*, Phys. Rev. D **78**, 023529 (2008).
 - [25] A. Lewis, *et al.*, Astrophys. J., **538**, 473 (2000).
 - [26] D. S. Salopek & J. R. Bond, PRD **42**, 3936 (1990).
 - [27] S. Furlanetto, *et al.*, Astrophys. J. **613**, 1 (2004).
 - [28] M. G. Santos, *et al.*, MNRAS **406**, 2421 (2010).

- [29] <http://www.simfast21.org>
- [30] S. Matarrese, *et al.*, *Astrophys. J.* **541**, 10 (2000).
- [31] M. McQuinn, *et al.*, *Astrophys. J.* **653**, 815 (2006).
- [32] S. Wyithe & M. F. Morales, *arXiv:astro-ph/0703070*.